Size and Energy Level Tuning of Quantum Dot Solids via a Hybrid Ligand Complex

Marcus L. Böhm[†,], Tom C. Jellicoe[†], Jasmine P.H. Rivett[†], Aditya Sadhanala[†], Nathaniel J.L.K. Davis[†], Frederik S.F. Morgenstern[†], Karl C. Gödel[†], Jayamurugan Govindasamy[ϰ], Callum G.M. Benson[ϰ], Neil C. Greenham[†] and Bruno Ehrler[‡,*]*

[†] Cavendish Laboratory, University of Cambridge, J.J. Thomson Avenue, Cambridge CB3 0HE, United Kingdom

[ϰ] Department of Chemistry, University of Cambridge, Lensfield Road, Cambridge CB2 1EW, United Kingdom

[‡] Center for Nanophotonics, FOM Institute AMOLF, Science Park 104, 1098 XG Amsterdam, The Netherlands

ABSTRACT

The performance of quantum dots (QDs) in optoelectronic devices suffers as a result of sub-bandgap states induced by the large fraction of atoms on the surface of QDs. Recent progress in passivating these surface states with thiol ligands and halide ions has led to competitive efficiencies. Here we apply a hybrid ligand mixture to passivate PbSe QD sub-bandgap tail states

via a low-temperature, solid-state ligand exchange. We show that this ligand mixture allows tuning of the energy levels and the physical QD size in the solid state during film formation. We hereby present a novel, post-synthetic path to tune the properties of QD films.

TABLE OF CONTENT GRAPHIC

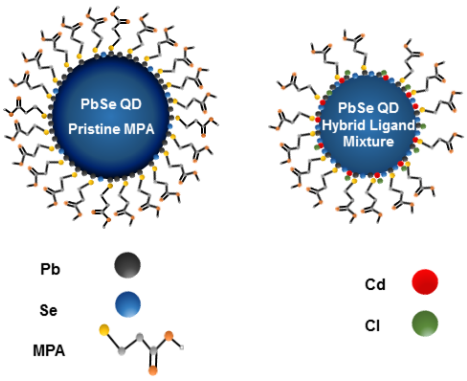

MAIN TEXT

In recent years quantum dots (QDs) have gathered interest for use in photodetectors,[1,2] LEDs,[3,4] and solar cells,[5,6] which have seen a surge in efficiency to almost 10%.[7] QDs are attractive because their properties (bandgap, processability, energy levels, doping levels) can be finely tuned, by tailoring their size and surface chemistry.[8–10] For example, the application of halide species as surface passivating agents has enabled the fabrication of high-performing QD-based optoelectronic devices[6,11–13] and also increased their stability in ambient environments.[7,14] Most of these reports rely on a successive solution/solid-state approach where the halide is provided *via* a metal salt during the QD synthesis and the remaining native ligands (most often oleic acid) are replaced by short, bidentate molecules during film deposition.[11,15] The surface passivation in these mixed solution/solid-state methods, however, still remains highly dependent

on the QD synthesis conditions. Furthermore, selective energy level tuning can sometimes only be achieved by elaborate methods such as vacuum evaporation[16] or the choice of different surface ligands.[7,8]

Here we present a robust QD passivation method where a hybrid ligand solution is applied to replace the native ligands during the QD film deposition. The ligand mixture consists of $CdCl_2$ and MPA, which are in equilibrium with a Cd-MPA metal-organic complex. Employing nuclear magnetic resonance spectroscopy, electron microscopy and a range of X-ray techniques we show that the QD Fermi level, physical size, and thereby the bandgap, can be controlled simultaneously by changes of the ratio of the components in the hybrid ligand mixture. We also find reduced density of sub-bandgap trap states, beneficial for optoelectronic devices.

We coordinate 3-mercaptopropionic acid (MPA) ligands to Cd by adding $CdCl_2$ to a methanolic solution of MPA. To study the coordination between MPA and Cd we employ nuclear magnetic resonance (^{1}H-NMR) spectroscopy on ligand samples containing molar percentages of $CdCl_2$ in the hybrid ligand mixture ranging from 0 mol% to 50 mol% (see **Figure 1**(a)). The triplet signals around 2.6 ppm and 2.7 ppm in pure MPA (red curve) can be assigned to the chemical equivalent protons vicinal to the carboxylate and thiol group. The partial coordination to Cd produces a second pair of triplets, which is shifted downfield to the respective free MPA triplet resonance. We identify a broadened thiol resonance in ^{1}H-NMR at ca. 1.9 ppm which is in agreement with literature reports suggesting a Cd-MPA coordination through the thiol group of MPA (Figure 1(a)).[9,17–21] The predominant coordination of MPA to Cd has been found to be through a non-chelating, dithio complex in aqueous solution.[17] In the remainder of

this article we assume a similar coordination in a comparably polar, protic solvents such as the methanol used here.

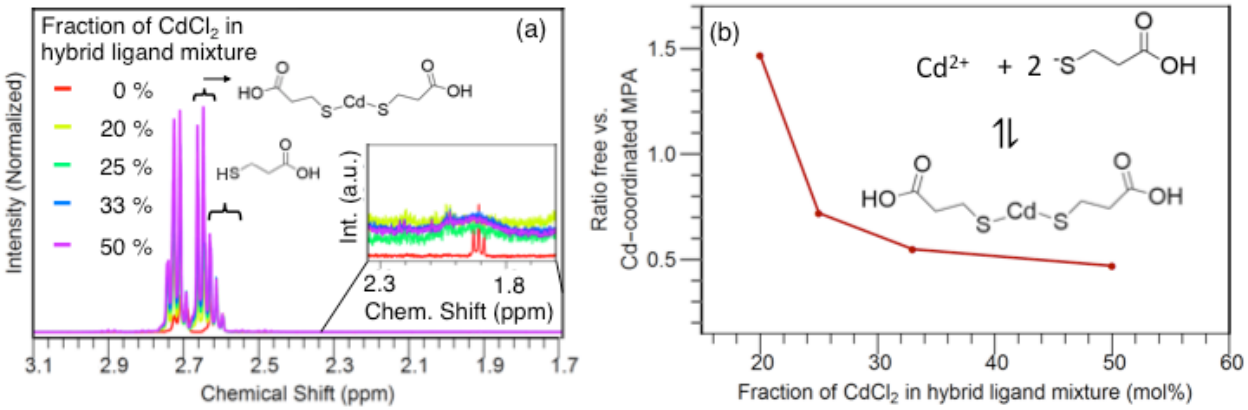

***Figure 1**. **(a)** [1]H nuclear magnetic resonance ([1]H NMR) spectra of samples with varying precursor ratio (the spectral region of the thiol proton is magnified in the inset). **(b)** Ratio of free vs. coordinated MPA extracted from the NMR data.*

To estimate the thermodynamic stability of the Cd-MPA complex we examine the spectral region of the triplet resonances from the vicinal protons to the thiol and carboxylate groups of MPA (ca. 2.7 ppm and 2.6 ppm respectively; see Figure 1(a)). Comparing the signals of MPA coordinated to Cd and free MPA allows us to determine the fraction of uncoordinated MPA in solution (see Figure 1(b) and Supporting Information S2). Based on this ratio we calculate the standard Gibbs free energy $\Delta G^{\ominus}$ for the coordination between Cd and MPA using the percentage of remaining uncoordinated MPA as a function of $CdCl_2$:MPA ratio. We estimate a $\Delta G^{\ominus}$ of ca. -16 kJ/mol suggesting spontaneous complex formation in solution (see Supporting Information S2). We do not find any precipitate forming even for the sample containing 50 mol% MPA in the $CdCl_2$:MPA mixture. We hence conclude at this stage that the hybrid ligand

mixture of $CdCl_2$ and MPA is in equilibrium with a Cd-MPA complex in solution and all species (i.e. residual reactants and complex) may act as QD ligands once deposited in a film. We will next evaluate the impact of the hybrid ligand mixture on QD film properties.

PbSe QDs ligated with oleic acid were synthesized following literature methods (see Supporting Information S1).[22] The particles were deposited in films using a layer-by-layer deposition technique[23,24] by spin-coating a QD film and exchanging the native ligand with the hybrid ligand mixture or pure MPA in a second spin-coating step. We then applied consecutive spin-rinsing steps using acetonitrile and octane. This process was repeated until the desired film thickness was reached. Absorption spectra of the QD films reveal a blue-shift of the first excitonic peak with increasing $CdCl_2$ concentration in the hybrid ligand mixture (see Supporting Information S3). Employing a size-bandgap correlation curve[10] we observe a reduction in particle diameter from 2.5 nm (pure MPA) to 2.1 nm (67 mol% MPA in the hybrid ligand mixture). Transmission electron microscopy (TEM) measurements corroborate the decrease in QD size with decreasing MPA loading in the hybrid ligand mixture showing a statistically significant difference in particle size between pure MPA and hybrid ligand treated samples (see **Figure 2**(a) and Supporting Information S3 and S4). Furthermore, we find that the particle size is relatively constant for the higher $CdCl_2$ fractions and only increases significantly for the pure MPA sample.

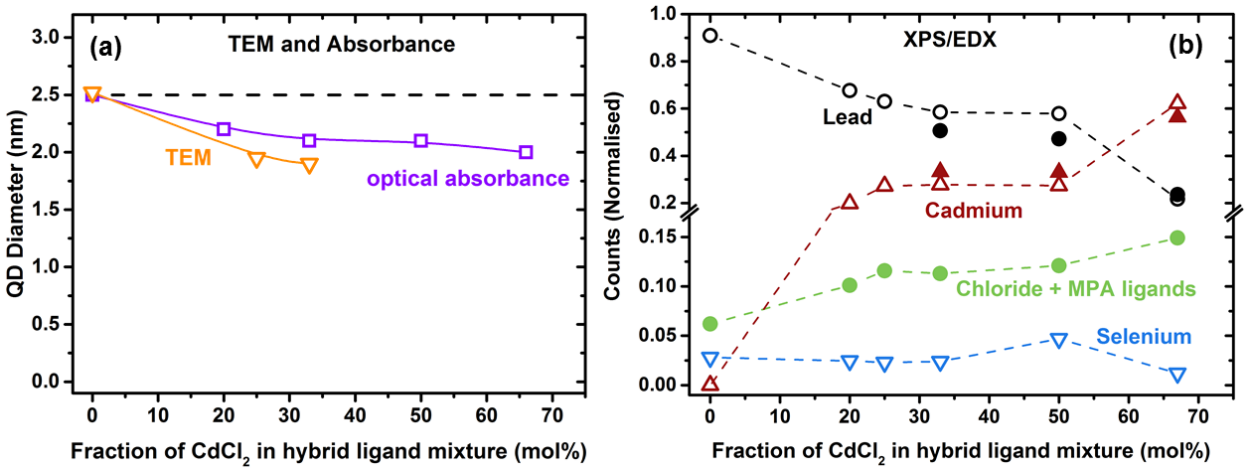

Figure 2: (a) *The change in PbSe QD diameter depending on the fraction of $CdCl_2$ in the hybrid ligand was determined by TEM and optical absorbance.* ***(b)*** *Analysis of the elemental constitution of PbSe QD films upon treatment with varying hybrid ligand concentration using X-ray photoelectron spectroscopy (XPS, open symbols) and energy dispersive X-ray (EDX, full symbols) measurements.*

It has been shown previously that the surface of small lead chalcogenide QDs consists predominantly of lead atoms.[25–28] It follows that the reduction in particle size is likely to decrease the relative Pb elemental contribution. Furthermore, we expect the overall ligand contribution to increase with smaller particles due to the increased surface-to-volume ratio. Indeed, monitoring the elemental contribution of Pb via X-ray photoelectron spectroscopy (XPS) and energy dispersive X-ray spectroscopy (EDX) revealed a decreased Pb signal intensity with higher $CdCl_2$ loadings in the hybrid ligand mixture (see Figure 2(b) and Supporting Information S5 and S6 for analysis). The almost constant Se signal as well as an increasing contribution of the ligand species Cl[11] and MPA (monitored through its distinct sulphur signal) are in agreement with a reduction in QD dimensions with increasing $CdCl_2$:MPA ratio. We note that in the XPS measurement, the normalized signal intensity of each element for of a given hybrid ligand

concentration does not reflect the relative elemental ratio due to the unknown and strongly element-specific X-ray absorption cross-section.[29] A more quantitative analysis would be possible using techniques such as diffusion-ordered NMR spectroscopy (DOSY-NMR).[30]

The reduction in QD dimensions and the role of the Cd-MPA complex therein can be understood by considering labile surface metal ions which reversibly bind to and dissociate from the QD surface through a metal-ligand complex.[21] In solution this process is governed by a Z-type ligand (i.e. electron-accepting metal-organic complex) displacement moderated through an L-type ligand species (i.e. a neutral, two electron-donating Lewis base)[31] which rapidly produces an equilibrium between bound and dissolved metal complex. In our solid-state approach where we apply an L-type ligand as rinse solvent (acetonitrile) we suggest that a similar mechanism is in operation. We conduct XPS measurements to analyze the lead and cadmium content of the acetonitrile spin-rinse solution for samples that were treated either with pristine MPA ligand or a hybrid ligand mixture (50 mol% $CdCl_2$; see **Figure 3**(a) and Supporting Information S1). The pure MPA ligand produces a solute without measurable residual cations, which is consistent with unchanged QD dimensions. This finding is in agreement with literature results.[32] In samples treated with the hybrid ligand mixture, however, we find clear evidence of lead and large amounts of cadmium in the acetonitrile rinse solution. Considering the large excess of Cd detected in the acetonitrile solute we suggest a mechanism where the hybrid ligand initially dilutes the desorbed Pb-complex thus suppressing re-adsorption. Due to the good solubility of the Cd-complex in acetonitrile (see Figure 3(b)) we furthermore argue that the following spin-rinse also prevents an extensive re-absorption of Cd on the particle surface which is consistent with the observed reduction in particle dimensions (see Figure 2(a)).

The equilibrium between de- and re-absorption of the metal complex which influences the surface stoichiometry has been shown to be highly sensitive to the presence of Lewis bases but less dependent on the metal complex concentration.[21] We therefore assign the drop and subsequently constant QD dimensions as a function of $CdCl_2$:MPA ratio (see Figure 3(a)) with

an initial turn-on of the Z-type ligand displacement mechanism due to the presence of the Cd-MPA complex. The displacement, then reaches an equilibrium at higher MPA loadings in the hybrid ligand mixture. The concentration of acetonitrile remains constant for all hybrid ligand constitutions and thus triggers the desorption of the same quantity of Pb-complexes from the QD surface for all $CdCl_2$:MPA ratios applied.

Beside the surface cation displacement mechanism we have to consider side reactions on the QD surface due to the reactive species that are present in the hybrid ligand mixture. For instance, the coordination of MPA to Cd produces hydrochloric acid which can catalyze the solid-state ligand exchange from native oleic acid ligands to MPA capping groups[19] and it is capable of etching QD surfaces within minutes.[33] While the first effect can be considered as beneficial for a ligand exchange reaction, we argue that the latter mechanism can be neglected since we do not observe a spectral change in optical absorbance in samples where the pure MPA ligand solution was blended with small quantities of HCl which is in agreement with unchanged particle dimensions (see Supporting Information S7). Note that the remaining Cl ions may also serve as an efficient passivation agent.[11,15,34] At high $CdCl_2$ loadings (>50mol% $CdCl_2$:MPA) another side reaction can be caused by residual, atomic-sized Cd clusters in the ligand mixture (see Supporting Information S8). Furthermore, we neglect the built-up of an alloyed QD due to the significant mismatch between the two crystal structures.[35] We finally consider as potential side reaction the formation of a core-shell structure where the lead atoms on the particle surface are replaced by Cd. While we cannot entirely exclude the formation of at least an incomplete Cd shell around the PbSe core from XRD or high-resolution TEM measurements alone (see supporting Information S9 and S10), we note that such Cd-lead chalcogenide core shell particles have only been demonstrated when fabricated in a post-synthetic solution approach at elevated

temperatures. We furthermore note that these QDs have been shown to preserve their initial diameter as the underlying mechanism proceeds via a Pb to Cd cation exchange reaction which is triggered from the QD surface.[24,36] We therefore suggest that our solid-state hybrid ligand treatment reduces the particle size predominantly through a surface cation-displacement mechanism and provides a mixed QD surface coverage with MPA, Cl, and Cd-species (see Figure 3(c)).

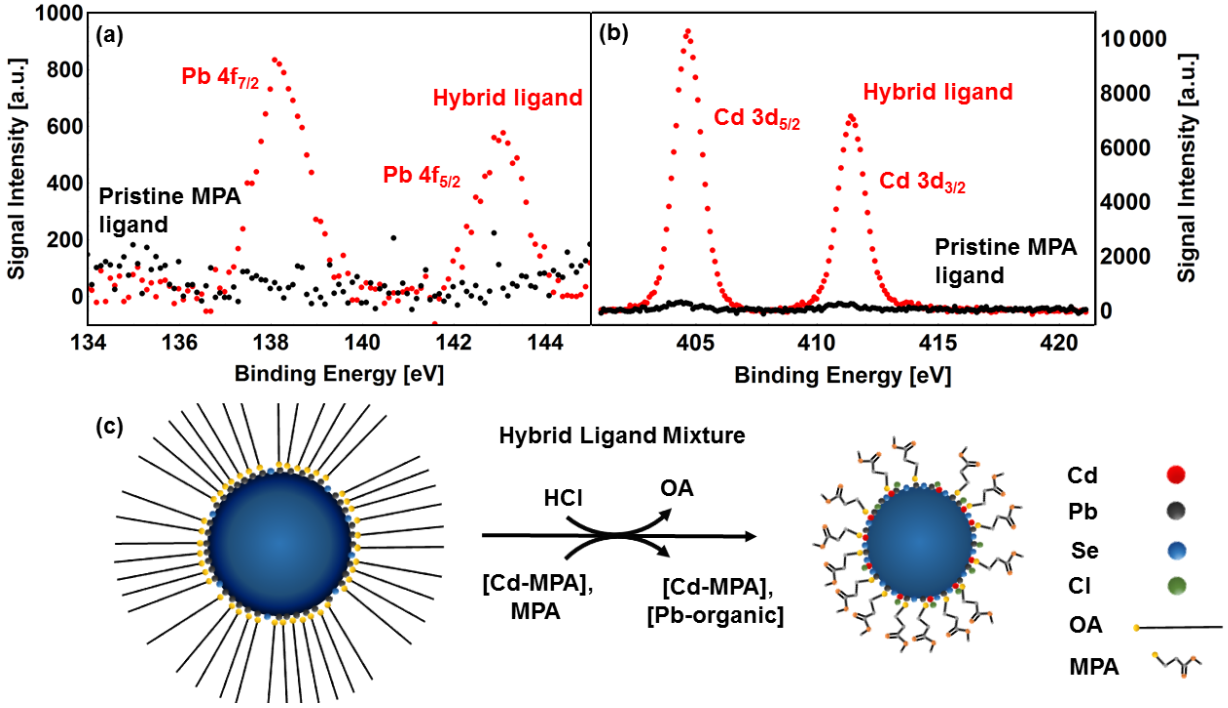

Figure 3: *(a) Lead and (b) cadmium XPS signals for acetonitrile rinse solutes after treatment with a hybrid ligand mixture (50 mol% MPA; red) and a pure MPA ligand (black). (c) Schematics of the acetonitrile initiated, Z-type ligand displacement of labile Pb surface ions.*

Treating QDs with $CdCl_2$ during the final phase of their synthesis has proven to be beneficial for optoelectronic devices as it reduces the trap state density, and allows tuning of the energy level alignment.[11,15] We determined the relevant energy levels within the QD film using a

combination of ultraviolet-photoelectron spectroscopy (UPS) and absorbance spectroscopy[37,38] (Supporting Information S3 and S11). We find that the energy of the QD valence band with respect to the vacuum level changes from -4.9 eV for the pure MPA ligand to -5.3 eV for samples with low $CdCl_2$ loading and returns to -5.0 eV for the sample with 67 mol% $CdCl_2$ content in the $CdCl_2$ MPA mixture (see **Figure 4**(a)). This shift towards lower valence band energies has been observed before when halide species are used for QD passivation.[7,8] In addition to the valence band shift, we also observe a shift in the Fermi level energy, indicating significant differences in carrier concentration. With higher $CdCl_2$ loading, the QD films become significantly more *n*-type, which is consistent with halide doping by the Cl species.[7,8] Determining the Urbach Energy E_U as a measure of the sub-bandgap state density using photothermal deflection spectroscopy (PDS) we find small, but detectable changes in the trap state density of PbSe QD films as a function of $CdCl_2$ concentration in the hybrid ligand mixture (see Figure 4(b)). This change can be rationalized by considering the passivation of trap states residing at the QD surface by Cd and Cl.[11,15] Note that the formation of the hybrid ligand complex prior to film deposition is necessary to reduce the quantity of sub-bandgap tail states as a sequential deposition of $CdCl_2$ and MPA does not lead to a decrease in E_U (see green data-points inset Figure 4(b) and Supporting Information S13).

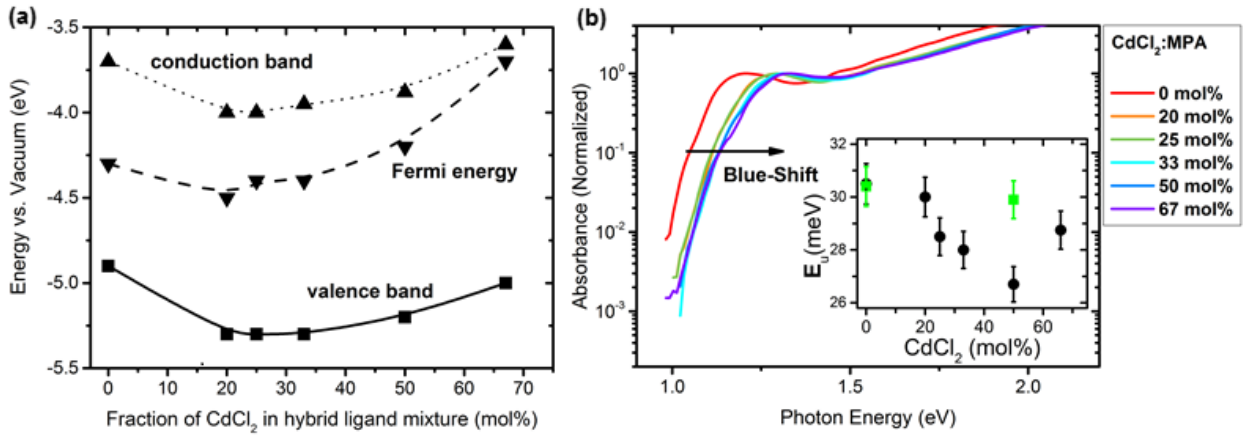

Figure 4 (a) *Conduction- and valence band energy as well as Fermi energy for PbSe QD films as a function of $CdCl_2$ in the hybrid ligand mixture.* ***(b)*** *Absorbance spectra of QD films measured with photothermal deflection spectroscopy. The inset shows the Urbach Energy (E_U), a measure of the sub-bandgap tail state density (green squares denote E_U of a QD film where the $CdCl_2$ was placed on the sample without the coordination to MPA).*

In conclusion we present a simple QD solid-state treatment using a hybrid ligand solution containing $CdCl_2$ and 3-mercaptopropionic acid (MPA). We show that the inorganic salt and the organic ligand are in equilibrium with a metal-ligand complex in solution. When this solution is employed as a ligand in the solid state we find a stronger quantum confinement due to a smaller QD core diameter, a deeper valence band energy, a shallower Fermi level, and a reduced quantity of sub-bandgap tail states. The ability to control band energies and Fermi levels in quantum dot films enables new opportunities for post-synthetic band engineering (e.g. “quantum-junction” structures[39]) for solution-processed solar cells based on a single batch of quantum dots.

ASSOCIATED CONTENT

Supporting Information. Materials characterization, film formation, and experimental details can be found in the Supporting Information. This material is available free of charge via the Internet at http://pubs.acs.org.

AUTHOR INFORMATION

Corresponding Authors

*Email: mb842@cam.ac.uk, b.ehrler@amolf.nl

Author Contributions

The manuscript was written through contributions of all authors. All authors have given approval to the final version of the manuscript.

Notes

The authors declare no competing financial interests.

ACKNOWLEDGMENT

M.L.B thanks the German National Academic Foundation (Studienstiftung) for funding. This work was supported by the Engineering and Physical Sciences Research Council [Grant number EP/G060738/1 and Cambridge NanoDTC, EP/G037221/1].

REFERENCES

(1) Konstantatos, G.; Levina, L.; Fischer, A.; Sargent, E. Engineering the Temporal Response of Photoconductive Photodetectors via Selective Introduction of Surface Trap States. *Nano Lett.* **2008**, *8*, 1446.

(2) Sukhovatkin, V.; Hinds, S.; Brzozowski, L.; Sargent, E. H. Colloidal Quantum-Dot Photodetectors Exploiting Multiexciton Generation. *Science* **2009**, *324*, 1542–1544.

(3) Kwak, J.; Lim, J.; Park, M.; Lee, S.; Char, K.; Lee, C. High-Power Genuine Ultraviolet Light-Emitting Diodes Based On Colloidal Nanocrystal Quantum Dots. *Nano Lett.* **2015**, *15*, 3793.

(4) Mutlugun, E.; Guzelturk, B.; Abiyasa, A. P.; Gao, Y.; Sun, X. W.; Demir, H. V. Colloidal Quantum Dot Light-Emitting Diodes Employing Phosphorescent Small Organic Molecules as Efficient Exciton Harvesters. *J. Phys. Chem. Lett.* **2014**, *5*, 2802–2807.

(5) Luther, J. M.; Gao, J.; Lloyd, M. T.; Semonin, O. E.; Beard, M. C.; Nozik, A. J. Stability Assessment on a 3% Bilayer PbS/ZnO Quantum Dot Heterojunction Solar Cell. *Adv. Mater.* **2010**, *22*, 3704–3707.

(6) Crisp, R. W.; Kroupa, D. M.; Marshall, A. R.; Miller, E. M.; Zhang, J.; Beard, M. C.; Luther, J. M. Metal Halide Solid-State Surface Treatment for High Efficiency PbS and PbSe QD Solar Cells. *Sci. Rep.* **2015**, *5*, 9945.

(7) Chuang, C.; Brown, P.; Bulović, V.; Bawendi, M. Improved Performance and Stability in Quantum Dot Solar Cells through Band Alignment Engineering. *Nat. Mater.* **2014**, *13*, 796–801.

(8) Brown, P. R.; Kim, D.; Lunt, R. R.; Zhao, N.; Bawendi, M. G.; Grossman, J. C.; Bulovi, V. Energy Level Modification in Lead Sulfide Quantum Dot Thin Films through Ligand Exchange. *ACS Nano* **2014**, *8*, 5863–5872.

(9) Böhm, M. L.; Kist, R. J. P.; Morgenstern, F. S. F.; Ehrler, B.; Zarra, S.; Kumar, A.; Vaynzof, Y.; Greenham, N. C. The Influence of Nanocrystal Aggregates on Photovoltaic Performance in Nanocrystal-Polymer Bulk Heterojunction Solar Cells. *Adv. Energy Mater.* **2014**, 1400139.

(10) Jasieniak, J.; Califano, M.; Watkins, S. E. Size-Dependent Valence and Conduction Band-Edge Energies of Semiconductor Nanocrystals. *ACS Nano* **2011**, *5*, 5888–5902.

(11) Ip, A. H.; Thon, S. M.; Hoogland, S.; Voznyy, O.; Zhitomirsky, D.; Debnath, R.; Levina, L.; Rollny, L. R.; Carey, G. H.; Fischer, A.; *et al.* Hybrid Passivated Colloidal Quantum Dot Solids. *Nat. Nanotechnol.* **2012**, *7*, 577–582.

(12) Tang, J.; Kemp, K. W.; Hoogland, S.; Jeong, K. S.; Liu, H.; Levina, L.; Furukawa, M.; Wang, X.; Debnath, R.; Cha, D.; *et al.* Colloidal-Quantum-Dot Photovoltaics Using Atomic-Ligand Passivation. *Nat. Mater.* **2011**, *10*, 765–771.

(13) Marshall, A. R.; Young, M. R.; Nozik, A. J.; Beard, M. C.; Luther, J. M. Exploration of Metal Chloride Uptake for Improved Performance Characteristics of PbSe Quantum Dot Solar Cells. *J. Phys. Chem. Lett.* **2015**, *6*, 2892–2899.

(14) Ning, Z.; Voznyy, O.; Pan, J.; Hoogland, S.; Adinolfi, V.; Xu, J.; Li, M.; Kirmani, A. R.; Sun, J.-P.; Minor, J.; *et al.* Air-Stable N-Type Colloidal Quantum Dot Solids. *Nat. Mater.* **2014**, *13*, 822–828.

(15) Asil, D.; Walker, B. J.; Ehrler, B.; Vaynzof, Y.; Sepe, A.; Bayliss, S.; Sadhanala, A.; Chow, P. C. Y.; Hopkinson, P. E.; Steiner, U.; *et al.* Role of PbSe Structural Stabilization in Photovoltaic Cells. *Adv. Funct. Mater.* **2014**, *25*, 928–935.

(16) Oh, S. J.; Berry, N. E.; Choi, J. H.; Gaulding, E. A.; Paik, T.; Hong, S. H.; Murray, C. B.; Kagan, C. R. Stoichiometric Control of Lead Chalcogenide Nanocrystal Solids to Enhance Their Electronic and Optoelectronic Device Performance. *ACS Nano* **2013**, *7*, 2413–2421.

(17) Vairavamurthy, M. A.; Goldenberg, W. S.; Ouyang, S.; Khalid, S. The Interaction of Hydrophilic Thiols with Cadmium: Investigation with a Simple Model, 3-Mercaptopropionic Acid. *Mar. Chem.* **2000**, *70*, 181–189.

(18) Hassinen, A.; Moreels, I.; De Nolf, K.; Smet, P. F.; Martins, J. C.; Hens, Z. Short-Chain Alcohols Strip X-Type Ligands and Quench the Luminescence of PbSe and CdSe Quantum Dots, Acetonitrile Does Not. *J. Am. Chem. Soc.* **2012**, *134*, 20705–20712.

(19) Fritzinger, B.; Capek, R. K.; Lambert, K.; Martins, J. C.; Hens, Z. Utilizing Self-Exchange to Address the Binding of Carboxylic Acid Ligands to CdSe Quantum Dots. *J. Am. Chem. Soc.* **2010**, *132*, 10195–10201.

(20) Morris-cohen, A. J.; Malicki, M.; Peterson, M. D.; Slavin, J. W. J.; Weiss, E. A. Chemical, Structural, and Quantitative Analysis of the Ligand Shells of Colloidal Quantum Dots. *Chem. Mater.* **2013**, *25*, 1155.

(21) Anderson, N. C.; Hendricks, M. P.; Choi, J. J.; Owen, J. S. Ligand Exchange and the Stoichiometry of Metal Chalcogenide Nanocrystals: Spectroscopic Observation of Facile Metal-Carboxylate Displacement and Binding. *J. Am. Chem. Soc.* **2013**, *135*, 18536–18548.

(22) Murray, C. B.; Sun, S.; Gaschler, W.; Doyle, H.; Betley, T. A.; Kagan, C. R. Colloidal Synthesis of Nanocrystals and Nanocrystal Superlattices. *IBM J. Res. Dev.* **2001**, *45*, 47–56.

(23) Konstantatos, G.; Howard, I.; Fischer, A.; Hoogland, S.; Clifford, J.; Klem, E.; Levina, L.; Sargent, E. H. Ultrasensitive Solution-Cast Quantum Dot Photodetectors. *Nature* **2006**, *442*, 180–183.

(24) Neo, D. C. J.; Cheng, C.; Stranks, S. D.; Fairclough, S. M.; Kim, J. S.; Kirkland, A. I.; Smith, J. M.; Snaith, H. J.; Assender, H. E.; Watt, A. A. R. Influence of Shell Thickness and Surface Passivation on PbS/CdS Core/Shell Colloidal Quantum Dot Solar Cells. *Chem. Mater.* **2014**, *26*, 4004–4013.

(25) Dai, Q.; Wang, Y.; Li, X.; Zhang, Y.; Pellegrino, D. J.; Zhao, M.; Zou, B.; Seo, J.; Yu, W. W. Size-Dependent Composition and Molar Extinction Coefficient of PbSe Semiconductor Nanocrystals. *ACS Nano* **2009**, *3*, 1518–1524.

(26) Primera-Pedrozo, O. M.; Arslan, Z.; Rasulev, B.; Leszczynski, J. Room Temperature Synthesis of PbSe Quantum Dots in Aqueous Solution: Stabilization by Interactions with Ligands. *Nanoscale* **2012**, *4*, 1312–1320.

(27) Moreels, I.; Justo, Y.; Geyter, B. De. Size-Tunable, Bright, and Stable PbS Quantum Dots: A Surface Chemistry Study. *ACS Nano* **2011**, 2004–2012.

(28) Luther, J. M.; Pietryga, J. M. Stoichiometry Control in Quantum Dots: A Viable Analog to Impurity Doping of Bulk Materials. *ACS Nano* **2013**, *7*, 1845–1849.

(29) Scofield, J. H. Hartree-Slater Subshell Photoionization Cross-Sections. *J. Electron Spectros. Relat. Phenomena* **1976**, *8*, 129.

(30) Gomes, R.; Hassinen, A.; Szczygiel, A.; Zhao, Q.; Vantomme, A.; Martins, J. C.; Hens, Z. Binding of Phosphonic Acids to CdSe Quantum Dots: A Solution NMR Study. *J. Phys. Chem. Lett.* **2011**, *2*, 145–152.

(31) Green, M. L. H. A New Approach to the Formal Classification of Covalent Compounds of the Elements. *J. Organomet. Chem.* **1995**, *500*, 127–148.

(32) Kirmani, A. R.; Carey, G. H.; Abdelsamie, M.; Yan, B.; Cha, D.; Rollny, L. R.; Cui, X.; Sargent, E. H.; Amassian, A. Effect of Solvent Environment on Colloidal-Quantum-Dot Solar-Cell Manufacturability and Performance. *Adv. Mater.* **2014**, *26*, 4717–4723.

(33) Lv, Y.; Li, K.; Li, Y. Surface Modification of Quantum Dots and Magnetic Nanoparticles with PEG-Conjugated Chitosan Derivatives for Biological Applications. *Chem. Pap.* **2013**, *67*, 1404–1413.

(34) Tang, J.; Kemp, K. W.; Hoogland, S.; Jeong, K. S.; Liu, H.; Levina, L.; Furukawa, M.; Wang, X.; Debnath, R.; Cha, D.; *et al.* Colloidal-Quantum-Dot Photovoltaics Using Atomic-Ligand Passivation. *Nat. Mater.* **2011**, *10*, 765–771.

(35) Heiss, W.; Groiss, H.; Kaufmann, E.; Hesser, G.; Böberl, M.; Springholz, G.; Schäffler, F.; Leitsmann, R.; Bechstedt, F.; Koike, K.; *et al.* Quantum Dots with Coherent Interfaces between Rocksalt-PbTe and Zincblende-CdTe. *J. Appl. Phys.* **2007**, *101*, 081723.

(36) Neo, M. S.; Venkatram, N.; Li, G. S.; Chin, W. S.; Ji, W. Synthesis of PbS/CdS Core-Shell QDs and Their Nonlinear Optical Properties. *J. Phys. Chem. C* **2010**, *114*, 18037–18044.

(37) Ehrler, B.; Walker, B. J.; Böhm, M. L.; Wilson, M. W. B.; Vaynzof, Y.; Friend, R. H.; Greenham, N. C. In Situ Measurement of Exciton Energy in Hybrid Singlet-Fission Solar Cells. *Nat. Commun.* **2012**, *3*, 1019.

(38) Davis, N. J. L. K.; Böhm, M. L.; Tabachnyk, M.; Wisnivesky-Rocca-Rivarola, F.; Jellicoe, T. C.; Ducati, C.; Ehrler, B.; Greenham, N. C. Multiple Exciton Generation in Lead Selenide Nanorod Solar Cells with External Quantum Efficiencies Exceeding 120 %. *Nat. Commun.*

(39) Tang, J.; Liu, H.; Zhitomirsky, D.; Hoogland, S.; Wang, X.; Furukawa, M.; Levina, L.; Sargent, E. H. Quantum Junction Solar Cells. *Nano Lett.* **2012**, *12*, 4889–4894.

Synopsis

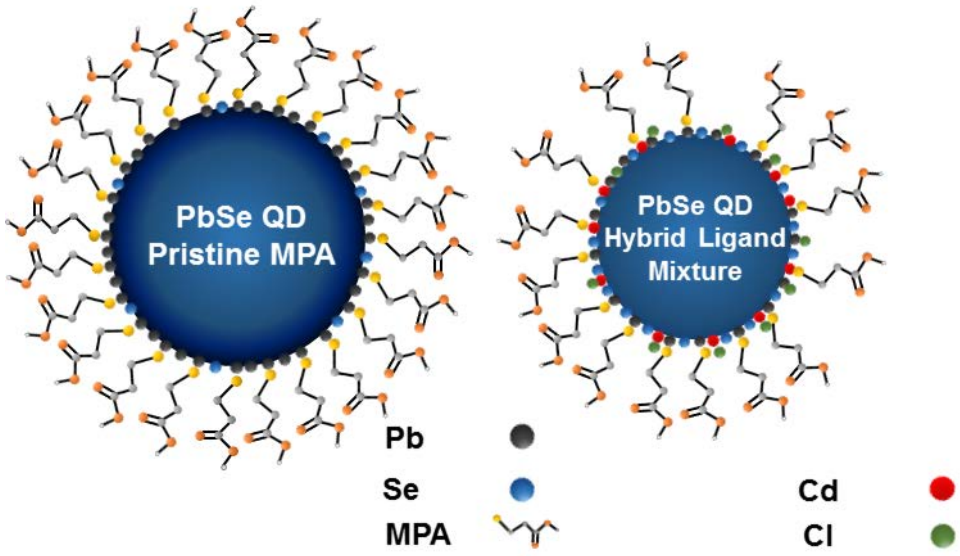

Supporting Information for

Size and Energy Level Tuning of Quantum Dot Solids via a Hybrid Ligand Complex

Marcus L. Böhm, Tom C. Jellicoe, Jasmine P.H. Rivett, Aditya Sadhanala, Nathaniel J. L. K. Davis, Frederik S.F. Morgenstern, Karl C. Gödel, Jayamurugan Govindasamy, Callum G.M. Benson, Neil C. Greenham and Bruno Ehrler

S1 – Methods

QD synthesis

PbSe QDs with a band gap ~ 1 eV were synthesised by a previously reported method.[1] In a typical synthesis 2.2 g lead acetate trihydrate ($Pb(OAc)_2 \cdot 3H_2O$) was added to 3.54 ml oleic acid (OA) in 34 ml 1-octadecene (ODE) and degassed at 110^{o}C under vacuum for 1 h to form a Pb-oleate complex. This was heated to 130 ^{o}C under nitrogen before injection of 16.2 ml of a 1 M selenium trioctylphosphine solution (Se:TOP) containing 161 µl diphenylphosphine (DPP). The reaction was allowed to cool for 1 min 15 s before quenching with a cold water bath. The QDs were purified by precipitating from solution by addition of ethanol and centrifugation at 4000 rpm for 5 mins before re-dispersing in 10 ml hexane and two further precipitations with a butanol/methanol mixture. The purified QDs were then re-dispersed in octane to a concentration of ~ 100 mg/ml and stored under Argon.

Hybrid ligand mixture preparation

Hybrid ligand mixtures were prepared by addition of $CdCl_2$ to a 20 mM 3-mercaptopropionic acid (MPA) methanol solution in the appropriate molar ratio and heating under nitrogen at 50 ^{o}C overnight. The solution was allowed to cool to room temperature before use in QD film deposition.

QD film formation

QDs were spin-coated in a nitrogen filled glovebox in a layer-by-layer deposition approach as developed by others.[2] The first layer consisted of QDs spun from 25 mg/mL solution in octane at 1500 rpm for 10 s after a 3 s wait. The same spinning conditions were used to spin the ligand or ligand mixture solution and spin-wash cycles with pure acetonitrile and octane.

Nuclear Magnetic Resonance (^{1}H NMR) Spectroscopy

NMR spectra were recorded at 298 K using Bruker Avance DPX 400 MHz, NMR spectrometer. ^{1}H spectra are referenced to the residual solvent peak. Deuterated methanol (CD_3OD) was obtained from Sigma Aldrich and used without any further purification. NMR Signals are reported in terms of chemical shift in ppm. Samples were prepared by dissolving ~ 5 mg $CdCl_2$ and MPA in the appropriate molar ratio in methanol-d_4 at 50 ^{o}C overnight.

Photoelectron Spectroscopy

For photoelectron spectroscopy 3 nm chromium and 80nm gold were thermally evaporated onto cleaned silicon substrates. The QDs were deposited in a layer-by-layer fashion as described above. The samples were then transferred into the vacuum chamber of a Thermo Scientific ESCALAB 250Xi X-ray Photoelectron Spectrometer (XPS) minimizing air exposure (about 10 s).

Ultraviolet photoelectron spectroscopy (UPS) measurements were performed using a double-differentially pumped He gas discharge lamp (He I radiation (hv=21.2 eV); pass energy 2 eV). In Section S11 the spectra are presented as a function of binding energy with respect to vacuum level. To determine the valence band edge of the individual samples we fit the leading edge of the first main peak

at the Fermi- and secondary cut-off edge[3] with a straight line and take the axis intercept as the measurement for the valence band energy. The error is derived from that fit.

X-ray photoelectron spectroscopy (XPS) was performed using an XR6 monochromated Al K_α X-ray source with an energy $h\upsilon$=1486.6 eV and a spot size of 650 μm. To prevent the samples from surface charging an Argon-ion flood gun was used. For data analysis of both UPS- and XPS spectra we used the software package "Thermo Avantage" (Thermo Fisher Scientific Inc., Waltham, USA). In order to study the chemical composition of the rinse acetonitrile solvent after deposition of the hybrid ligand mixture (see Figure 3s(a) and (b) in the main text) we drop casted the rinse solvent on plain silicon substrates and allowed the solvent to evaporate.

Energy Dispersive X-ray (EDX) Spectroscopy

Samples were prepared on blank silicon substrates and the spectra were recorded using a Leo Gemini 1530 VP scanning electron microscope (SEM) at low magnification operating at a voltage of 10 V using an X-ray detector from Oxford Instruments (Model 7426).

X- ray diffraction (XRD) spectroscopy

Samples were prepared on quartz substrates. Measurements were performed on a Bruker D8θ/θ spectrometer with a position sensitive detector (LynxEye) and graphite 2nd beam monochromator with Cu source (Kα radiation; λ=1.54 Å). The measurement setup was set to Bragg-Brentano parafocusing geometry in reflection mode over $10° \leq 2\theta \leq 80°$ choosing step sizes of $\Delta 2\theta = 0.03°$.

Optical Absorption

The absorption of our films and solutions was measured with a dual beam simultaneously passing through the sample and a blank using a PerkinElmer Lambda 9 UV-Vis-NIR spectrometer.

Transmission Electron Microscopy (TEM)

Samples were prepared by affixing a TEM grid (200 Mesh Cu, Agar Scientific) onto a glass substrate. A single layer of PbSe QDs was deposited from an octane solution (ca. 5 mg/ml) and was ligand exchanged with the ligand mixture solution following methods described above. The prepared TEM grid was then removed from the glass substrate and measured employing a FEI Tecnai F20-G2 FEGTEM at 200 kV for the High resolution images and HAADF STEM at 300 kV for determining the QDs size and standard deviation.

Size and size-distribution of the QDs were determined by fitting a Gaussian function to the size distribution histogram taken from TEM images containing more than 800 QDs for each of the four QD samples. The size distribution corresponds to the full width at half maximum of the fitted Gaussian. The histograms in Figure S2 were extracted using ImageJ.[4]

S2 - NMR Analysis

In order to study the Cd-MPA binding mode in the complex we examine the ^{1}H NMR spectrum in the region where the proton of the –SH group (1.6 – 2.3 ppm) and –COOH group (10 – 12 ppm) resonate (see Figure). We observe a –SH proton signal in all hybrid ligand mixtures and notice that the clear triplet resonance in pure MPA is broadened in all hybrid ligand samples. This can be due to the reduced rotational mobility of the ligand once the complex is formed which results in a broadening of the initial triplet signal.[5–9] The absence of a resonance for the –COOH proton in all samples can be explained by the significantly lower pK_a value of the –COOH proton in MPA compared to the NMR solvent d_4-MeOH.[10,11] Due to this pK_a difference we consider the initial carboxylic acid group as deprotonated. A coordination to Cd via the carboxylic acid group of MPA may also explain the absence of the –COOH proton resonance. We note, however, that no proton resonance can be observed in the pristine MPA sample either. We therefore argue that the –COOH proton cannot be used to either rule-out or confirm a

coordination via the carboxylate functionality of MPA. Considering the broadened –SH signal for the hybrid ligand mixture which is consistent with current literature reports for a Cd coordination via the –SH group[12], we however argue that a Cd-MPA coordination through the carboxylic acid group is less likely.

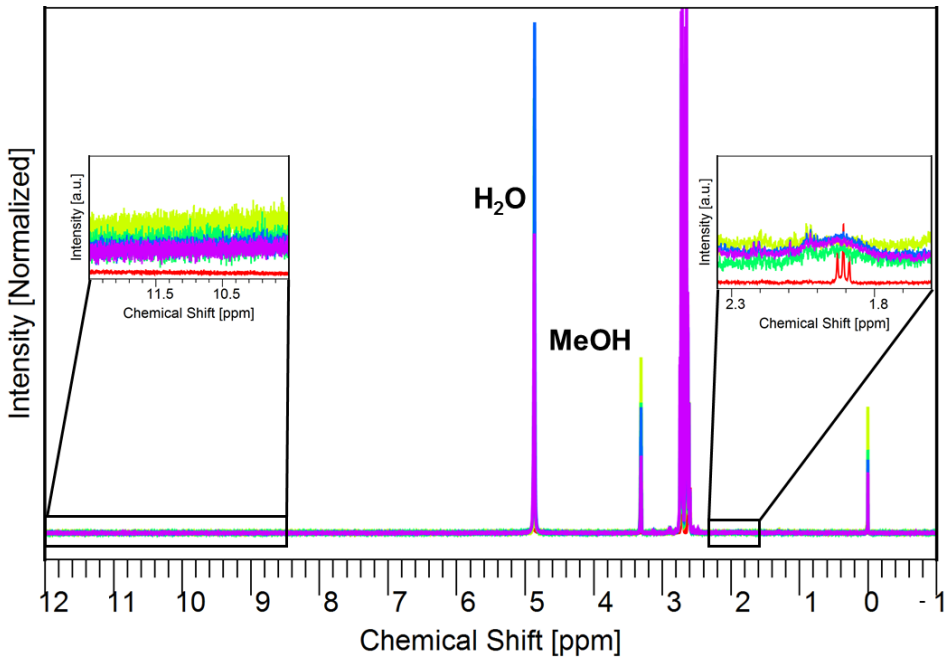

Figure S1: *Full ^{1}H NMR spectrum for the range of different hybrid ligands as shown in Figure 1 of the main text. The inset resolve the spectral regions where potential –COOH (10-12ppm) or –SH (1.6-2.3 ppm) are expected to resonate.*

In order to determine the standard Gibbs free energy of complex formation ($\Delta \boldsymbol{G}^{\ominus}$) we analyse the two triplet resonances at 2.61 and 2.71 ppm, which can be assigned to the two protons vicinal of the thiol and carboxylic functionality of pure MPA respectively. Upon coordination to Cd these triplets are shifted towards higher frequencies due to the electron withdrawing effect of Cd, coordinated to the sulphur group[12] (see Figure 1(a) in the main text).

By comparing the signal intensity of uncoordinated MPA with the resonances of coordinated MPA we calculate the ratio between uncoordinated and to Cd coordinated MPA (see Figure 1(a) in the main text).

For our analysis we only consider the area under the centre peaks of the respective triplet signals for coordinated (2.65 ppm) and uncoordinated MPA (2.61 ppm).

It has been shown that the dithio complex with one Cd coordinated to two MPA ligands is the most stable complex between Cd and MPA[12] but a different coordination is also conceivable. For the complex formation we therefore assume a dithio complex and the reactants to be in thermodynamic equilibrium according the equilibrium equation

$$Cd^{2+} + 2\,MPA^{-} \rightleftharpoons [MPA - Cd - MPA]$$

In order to estimate the standard Gibbs free energy $\Delta \boldsymbol{G}^{\ominus}$ for the formed dithio complex we first approximate the individual concentrations of complex and reactants in equilibrium. Note that we do not include a potential chelate complex into our considerations.[12] We take the initial concentrations of MPA and $CdCl_2$ and use the relation "Ratio free vs. Cd-coordinated MPA" as a function of the molar ratio between $CdCl_2$ and MPA (see Figure 1(b) in main text) to derive the concentrations of complex and reactants in equilibrium. We next calculate the dissociation constant $\boldsymbol{K_d}$ according the relation

$$K_d = \frac{[Cd^{2+}][MPA^{-}]^2}{[MPA - Cd - MPA]}$$

where $[Cd^{2+}]$, $[MPA^{-}]$ and $[MPA - Cd - MPA]$ are the concentrations of Cd-ions, uncoordinated MPA and complex in equilibrium. It follows the standard Gibbs free energy $\Delta G^{\ominus}$ which can be estimated using the equation

$$\Delta G^{\ominus} = -RT \ln \frac{K_d}{c^{\ominus}}$$

with *R*, *T* and $\boldsymbol{c}^{\ominus}$ being the ideal gas constant, temperature and standard reference concentration respectively. In a rough approximation we assume the standard Gibbs free energy $\Delta\boldsymbol{G}^{\ominus}$ to reach a plateau in our highest $CdCl_2$:MPA sample (50 mol%) and thus take the derived $\Delta\boldsymbol{G}^{\ominus}$ for this sample as our estimated binding affinity under the assumed conditions (dithio complex only, no chelate complex). The found ca. -16 kJ/mol (see Table S1) are consistent with literature reports for comparable metal-ligand binding affinities.[13]

Table S1. *Initial concentration of MPA and $CdCl_2$ as well as the concentrations of Cd, $MPA_{uncoordinated}$ and complex in equilibrium as a function of molar ratio between $CdCl_2$ and MPA. We also show the estimated dissociation constant K_d and standard Gibbs free energy $\Delta\boldsymbol{G}^{\ominus}$.*

$CdCl_2$:MPA [mol%]	**0**	**20**	**25**	**33**	**50**
Initial					
$[\boldsymbol{MPA}]_{\boldsymbol{total}}$ **[mM]**	218.6	218.6	164.0	109.3	54.4
$[\boldsymbol{CdCl_2}]_{\boldsymbol{total}}$ **[mM]**	-	54.4	54.4	54.4	54.4
In equilibrium					
$\frac{[\boldsymbol{MPA}]_{\boldsymbol{uncoordinated}}}{[\boldsymbol{MPA}]_{\boldsymbol{complex}}}$	-	1.49	0.72	0.55	0.47
$[\boldsymbol{MPA}]_{\boldsymbol{uncoordinated}}$ **[mM]**	218.6	130.0	68.7	38.8	17.4
$[\boldsymbol{Cd^{2+}}]_{\boldsymbol{uncoordinated}}$ **[mM]**	-	10.1	6.8	19.1	35.9
$[\boldsymbol{MPA-Cd-MPA}]$ **[mM]**	-	44.3	47.6	35.3	18.5
Thermodynamic Parameters					
Dissociation constant $\boldsymbol{K_d}$	-	$3.9\ 10^3$	669.2	816.3	588.9
Standard Gibbs free energy $\Delta\boldsymbol{G}^{\ominus}$ $[\frac{\boldsymbol{kJ}}{\boldsymbol{mol}}]$	-	- 20.5	-16.1	-16.6	-15.8

S3 – Transmission Electron Microscopy and Absorbance Spectroscopy

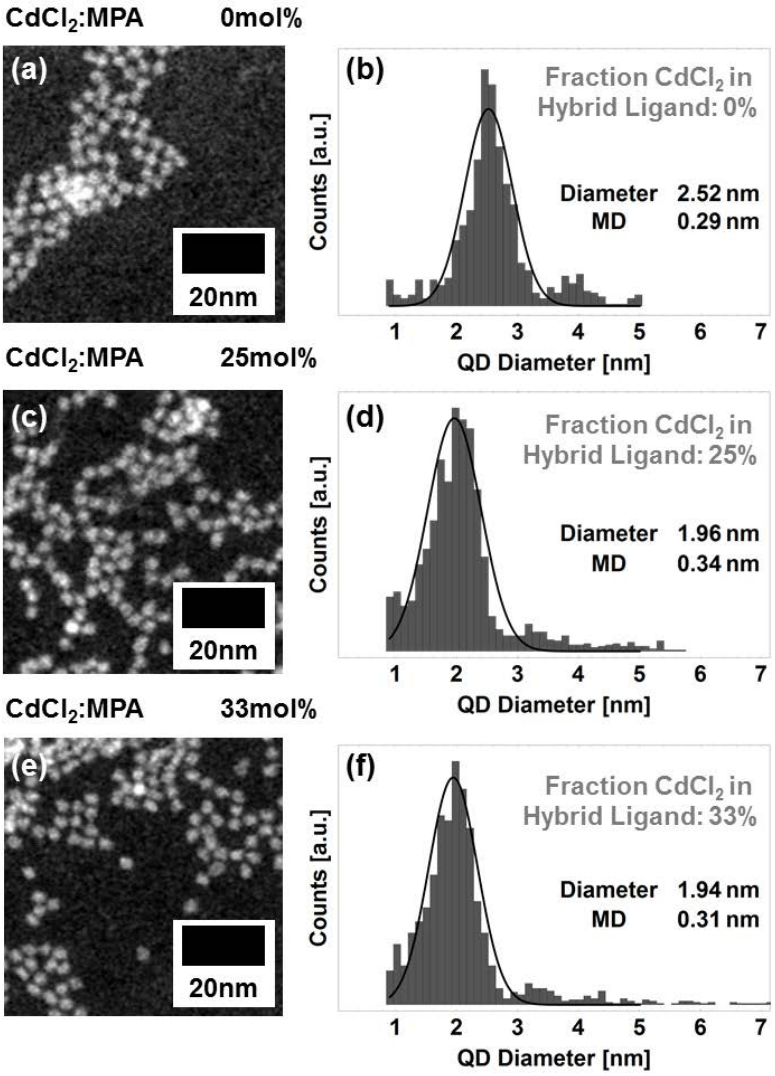

Figure S2 *Transmission electron microscopy images of PbSe QD films treated with a hybrid ligand mixture containing 0 % (a), 25 % (c) and 33 % (e) of $CdCl_2$. The corresponding particle diameter and particle mean distribution (MD) are determined by analysing more than 800 particles per sample (b,d,f).*

The measured value in Table S2 have been extracted from TEM histograms which considered more than 800 particles for each sample. The TEM images and the histograms are shown below.

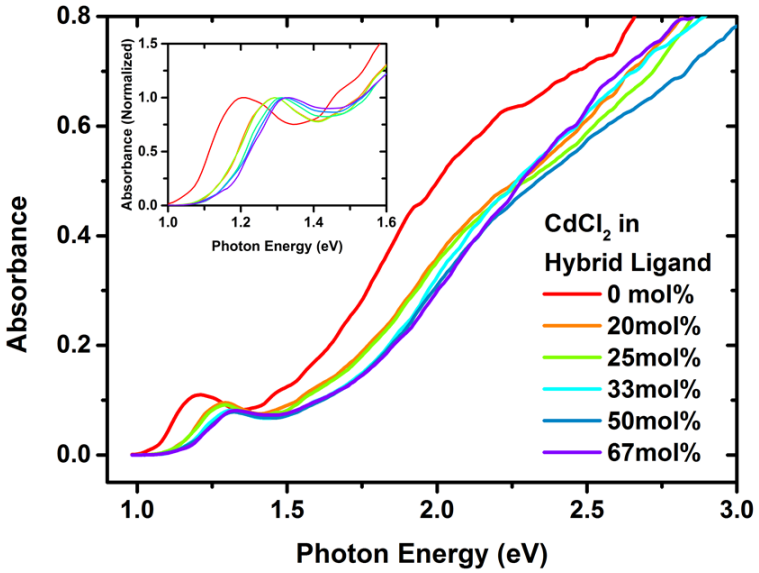

***Figure S3**: Absorption spectra for PbSe QD films which have been treated with different molar concentrations of a $CdCl_2$: MPA hybrid ligand solution.*

For our QD size estimation we assume in a first approximation a spherical QD shape, without any ligand. QD dimensions have been calculated by fitting a Gaussian function to the first excitonic peak in the absorbance spectrum according methods proposed by Jasieniak et al.[14] (see also Table S2).

***Table S2:** Measured and calculated values of QD diameter for samples treated with various ligand mixture ratios.*

$CdCl_2$:MPA ratio [mol%]	**QD Diameter [nm] -calculated from absorption-**	**QD Diameter [nm] -measured with TEM-**
0	2.5	2.52 ± 0.29
20	2.2	-
25	2.2	1.96 ± 0.34
33	2.1	1.94 ± 0.31
50	2.1	-
67	2.0	-

S4 – Testing for statistical difference for individual QD samples

QD areas were extracted from TEM images using ImageJ. QD diameters were estimated from QD areas by assuming spherical QDs. QD diameters were fitted with Gaussian distributions and a Welch's t-test was used to test the null hypothesis that the two distributions have equal means, without assuming that the two distributions also have equal variances. When the samples employing a hybrid ligand mixture of 33 mol% (Sample 33) and 25 mol% (Sample 25) of $CdCl_2$:MPA ratio were compared with the reference sample (0mol%), the null hypothesis was rejected at the 5% significance level. However, when Sample 33 was compared with Sample 25, the null hypothesis was accepted at the 5% significant level.

S5 – XPS Analysis

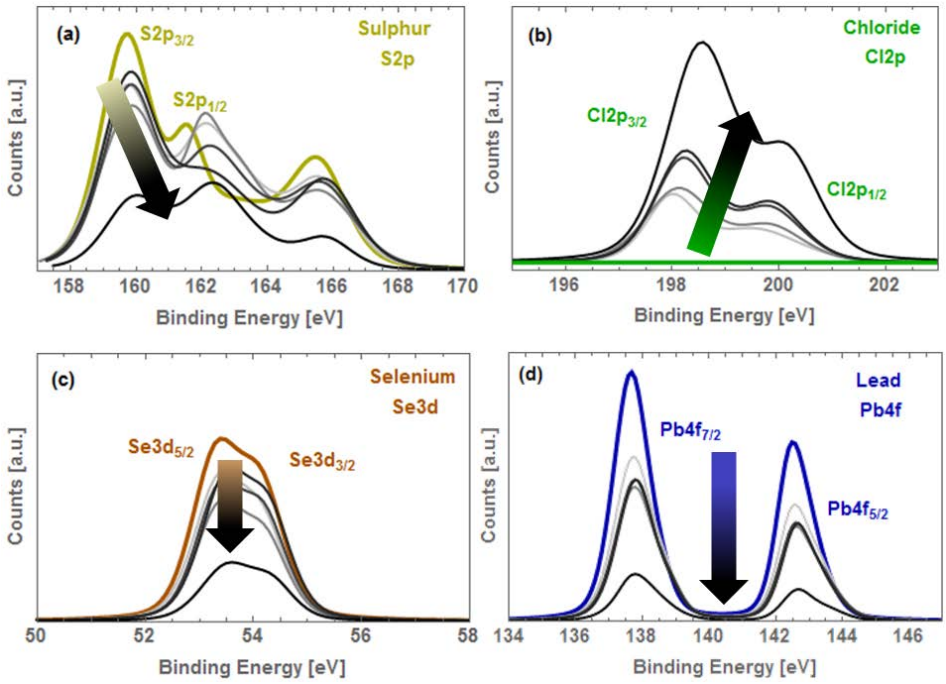

Figure S4. *Sulphur (a), chloride (b), selenium (c) and lead (d) X-ray photoelectron spectroscopy (XPS) analysis on PbSe QD films, which have been treated with a $CdCl_2$:MPA ligand mixture consisting of molar ratios between 0 mol% (colour) and 67 mol% (black). To underline the observable trend in single intensity caused by the different molar ratios of $CdCl_2$ to MPA we included arrows to guide the eye.*

In Figure and Figure (b), all spectra are shown in colour for 0 mol% CdCl2:MPA and an increasing grey value for $CdCl_2$:MPA molar concentrations of 20, 25, 33, 50 and 67 mol%. In the sulphur spectra (see Figure (a)) we identify a change in binding energy for the $S2p_{1/2}$ peak upon $CdCl_2$ introduction. This shift has also been observed for $CdCl_2$ treated PbS QDs and has been assigned to the changed binding environment of the MPA ligands, which have to compete for QD surface binding sites with present Cl atoms.[15] We furthermore notice, that the $Cd3d_{3/2}$ peak is superimposed on the Pb4d5 peak.

In order to quantify the change in elemental contribution of MPA, Cl and Se upon hybrid ligand treatment we integrate the respective peak intensities for each sample. Due to the overlapping $Cd3d_{3/2}$ and Pb4d5 signal we cannot simply integrate the peak area to quantify the cadmium content in our samples. We, however, note that the Pb4d5 contribution to the overall Cd3d signal only overlaps with the $Cd3d_{3/2}$ peak (see Figure). We therefore use the natural, relative ratio between the integral of the two Cd3d signals ($Cd3d_{5/2}$ / $Cd3d_{3/2}$ = 1.5)[16] and the absolute integral of the $Cd3d_{5/2}$ signal to determine the contribution of the Pb4d5 peak to the $Cd3d_{3/2}$ signal at each hybrid ligand ratio. After subtracting the Pb4d5 signal from the $Cd3d_{3/2}$ integral we add the resulting integral of both Cd3d signals ($Cd3d_{5/2}$ and $Cd3d_{3/2}$) to calculate the overall Cd3d integral. For the lead content we took the residual Pb4d5 contribution to the $Cd3d_{3/2}$ and added it to the integral of the whole Pb4f spectral region (Figure (d)).

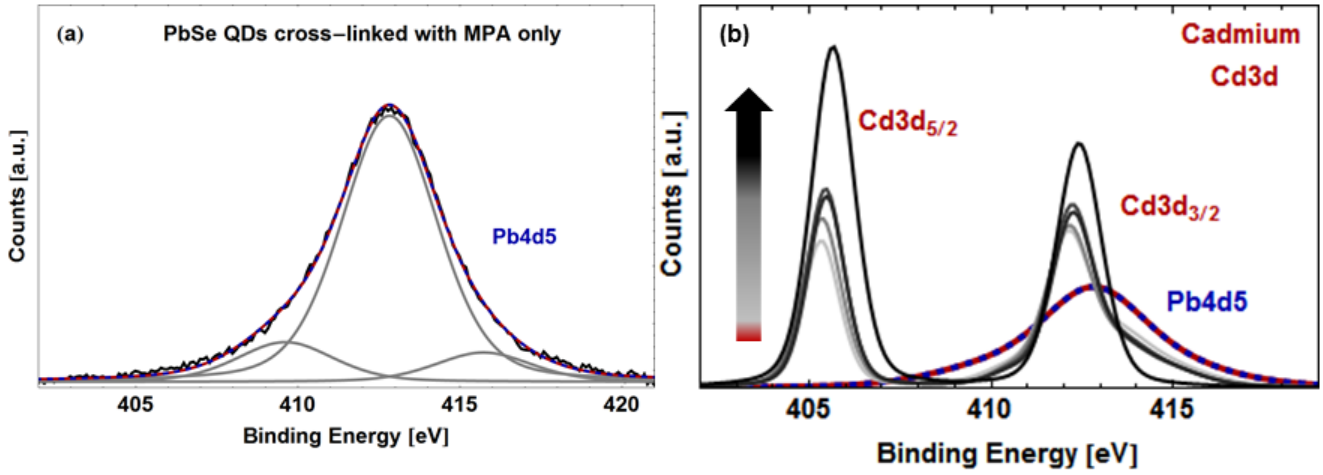

***Figure S5**. Quantification of abundant cadmium and lead using X-ray photoelectron spectroscopy (XPS) analysis.*

The relative atomic percentages are listed in Table S3.

Our XPS/EDX analysis of samples treated with 67 mol% of MPA in the hybrid ligand mixture reveal a Cd to MPA ratio of ca. 1:1 (see Table S3). This is in contradiction to our previous assumption of a dithio-complex (Supporting Information S2). As we observe a substantial amount of uncoordinated Cd in these samples (see Supporting Information S8) we, however, anticipate only part of the identified Cd to be included into the di-thio complex.

S6 – EDX Analysis

Atomic percentages of cadmium and lead have been measured using energy dispersive X - ray spectroscopy (EDX, see Figure). The significant signal at 1.8 eV stems from the silicon substrate on which the PbSe QDs have been deposited. We note that the used data software (INCA Energy, Oxford Instruments) has accounted for the overlapping Pb and Cl region using the difference in absorption cross-section of the different elements. The values from Figure (b) for Cd and from Figure (d) for Pb are listed in Table S3.

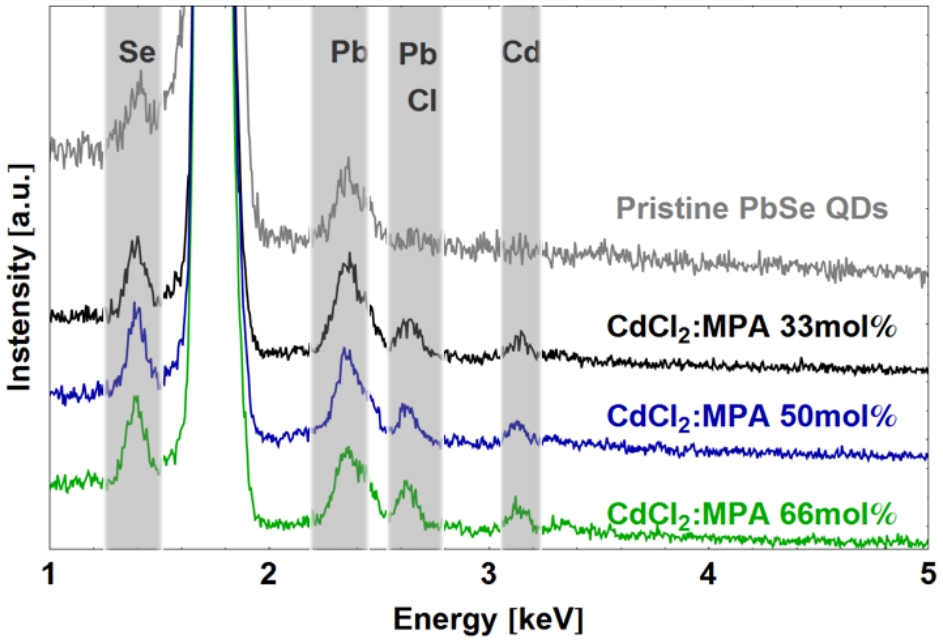

Figure S6. *Energy dispersive X-ray (EDX) spectra used for relative quantification of cadmium and lead in films of similar composition and thickness as shown for the XPS analysis (see Figure and Figure).*

We note that all values measured with EDX are within the 5% measurement error of the XPS values. Since the photon escape depth in EDX experiments is significantly larger than the electron escape depth in XPS, we can confirm that our XPS measurements are not limited by the inelastic mean free path length[17] of electrons escaping from the sample.

Table S3. *Summary of the atomic percentages derived via XPS and EDX on films of comparable composition and thickness.*

MPA in the hybrid ligand [mol%]	**0**	**20**	**25**	**33**	**50**	**66**
Cl	-	0.522	0.585	0.723	0.766	1.42
MPA	1	0.975	0.921	0.907	0.892	0.443
Σ Ligands	1	1.50	1.50	1.63	1.66	1.86
Cd	-	0.257	0.297	0.338/0.33*)	0.310/0.33*)	0.407/0.36*)
Pb	1	0.621	0.502	0.511/0.51*)	0.491/0.47*)	0.302/0.34*)
Se	1	0.796	0.650	0.764	0.824	0.321
Σ Pb,Se (Norm)	1	0.750	0.651	0.678	0.645	0.501

*) Measured quantities as determined by EDX.

S7 – Absorbance measurements of PbSe QDs in solution and after treatment with pure MPA in solid state

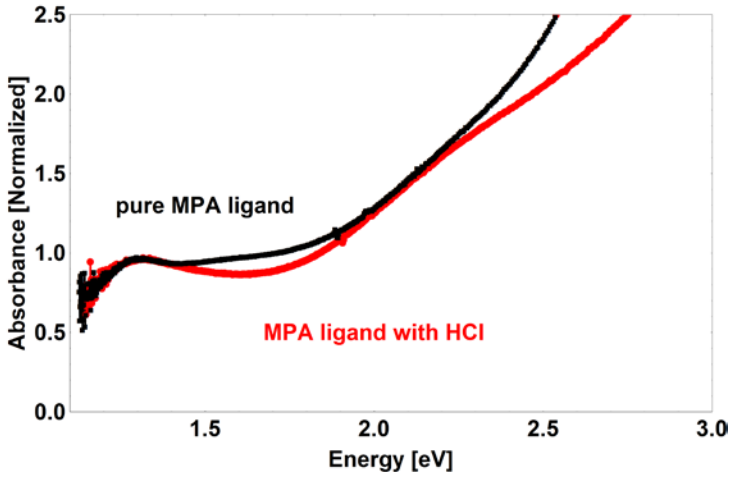

Figure S7. *Absorbance spectra of pure and HCl-modified MPA solutions which are employed as ligands during the layer-by-layer deposition of PbSe QDs.*

In the HCl modified sample HCl and MPA were mixed in equimolar quantities. No spectral shift can be observed compared to the reference sample.

S8 – TEM of PbSe QDs films employing 33 mol% MPA in the hybrid ligand mixture

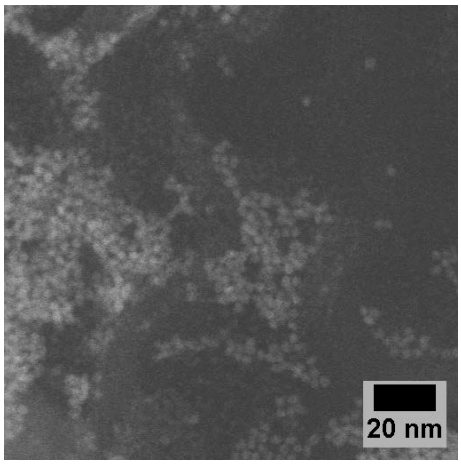

Figure S8. *Transmission Electron Microscope image of a PbSe QD film treated with 67 mol% of a $CdCl_2$ in the hybrid ligand solution.*

S9 – XRD analysis

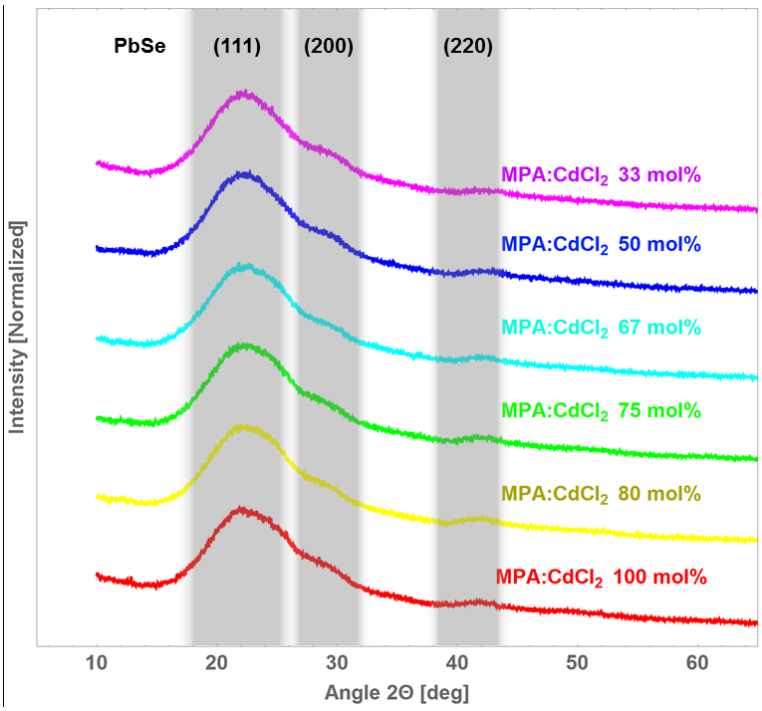

Figure S9. *X-ray diffraction (XRD) measurements of PbSe QDs treated with different molar ratios of a $CdCl_2$:MPA ligand solution. Only PbSe lattice features could be identified for all CdCl2:MPA ligand ratios.*[18]

S10 – High-resolution TEM images

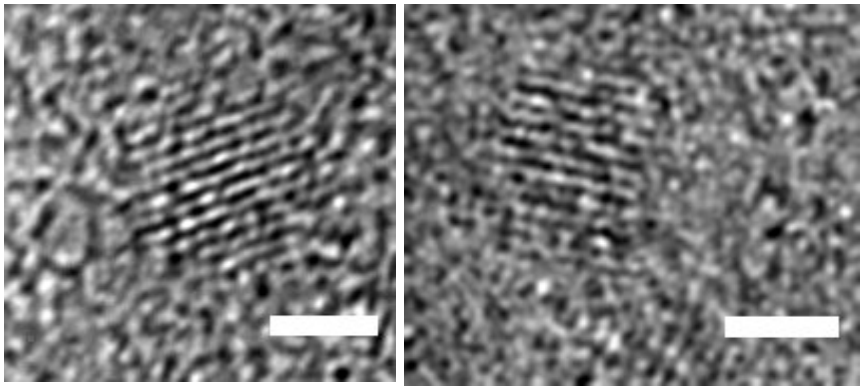

Figure S10. *High-resolution TEM images of pure MPA ligated (left) and hybrid ligand treated (33 mol% $CdCl_2$) PbSe QDs. The scale bars indicates 2nm.*

S11 – UPS Analysis

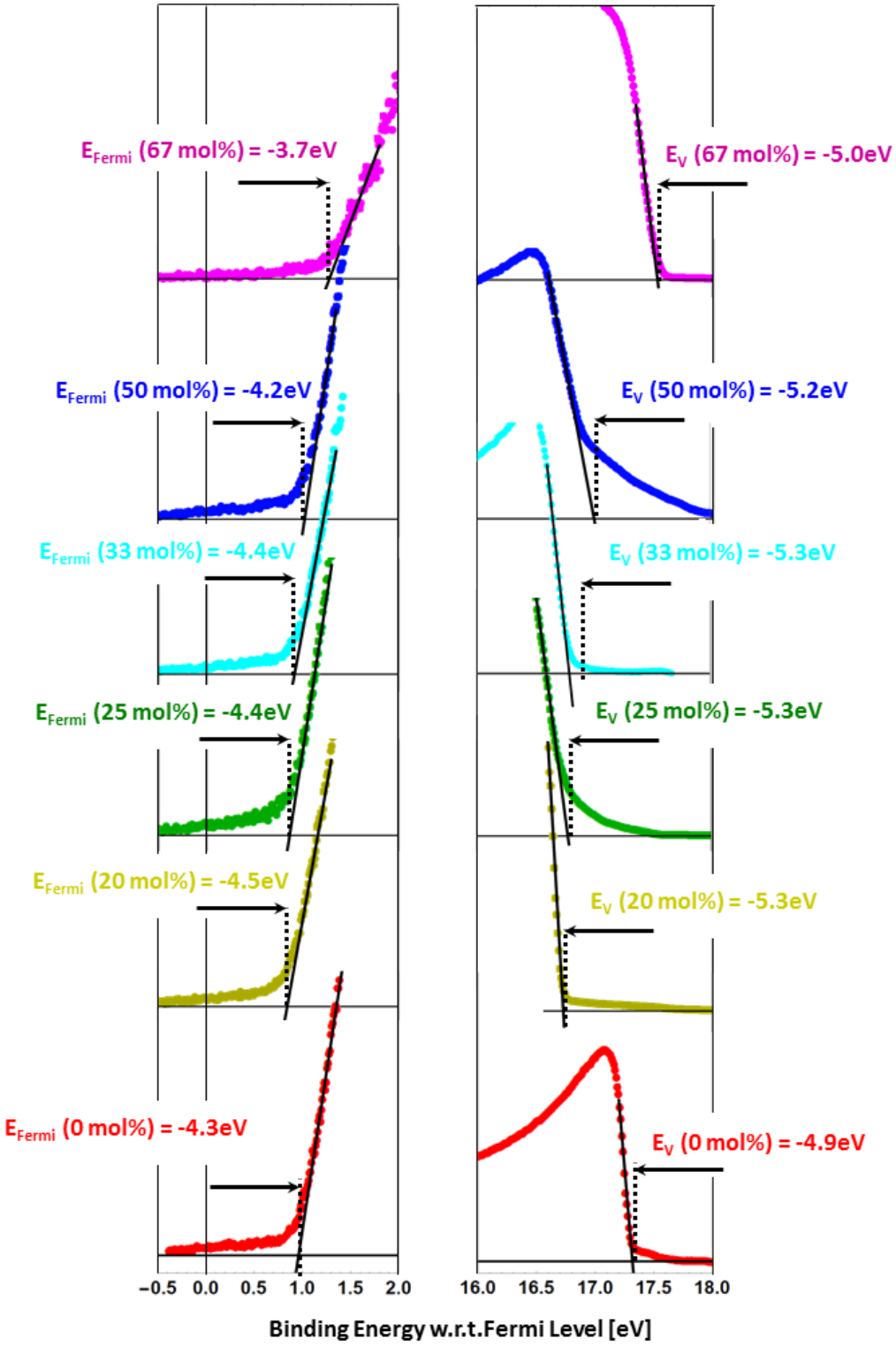

Figure S11. *Ultraviolet photoelectron spectroscopy (UPS) to determine the Fermi energy (E_{Fermi}) and valence band edge (E_V) of PbSe QDs treated with different molar ratios of MPA:$CdCl_2$ solution. The measurement error is 0.1 eV.*

S13 – Sequential deposition

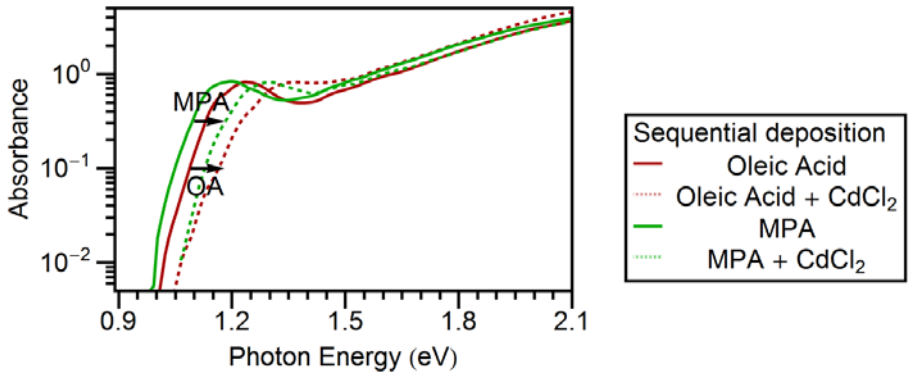

Figure S12. *PDS absorbance spectra of the QD films capped with oleic acid ligands and treated with $CdCl_2$ solution as well as QD films where the ligands were exchanged to MPA first and then treated with $CdCl_2$ solution.*

To gain mechanistic insight, and to show that the coordination of Cd to MPA is necessary to achieve the reduction in Urbach energy, we prepared QD films where MPA and $CdCl_2$ were applied sequentially. In the absence of MPA dimethylsulfoxide (DMSO) was used as the solvent to reach the required $CdCl_2$ solution concentration (20 mM) due to insufficient solubility in methanol. The absorbance of these films showed a similar blue-shift observed for pre-coordinated hybrid ligand mixtures, however, we do not observe a decrease in E_U (see inset Figure 4(b) in the main text and Supporting Information Figure S12). This suggests that the particle size is reduced in the sequential approach, but only the Cd-MPA hybrid ligand complex improves the QD surface passivation, potentially by offering a more sterically available QD surface.

$CdCl_2$ was dissolved in dimethylsulfoxide (DMSO) at 20 mM. Films for the sequential deposition of ligands and $CdCl_2$ were deposited as described above. In the first case, the native oleic acid ligands were preserved. The $CdCl_2$ solution was then placed on the film for 10 s before spinning. In the second case the ligands were first exchanged to MPA as above and then the same $CdCl_2$ treatment was applied.

References

(1) Ehrler, B.; Walker, B. J.; Böhm, M. L.; Wilson, M. W. B.; Vaynzof, Y.; Friend, R. H.; Greenham, N. C. In Situ Measurement of Exciton Energy in Hybrid Singlet-Fission Solar Cells. *Nat. Commun.* **2012**, *3*, 1019.

(2) Pattantyus-Abraham, A.; Kramer, I. Depleted-Heterojunction Colloidal Quantum Dot Solar Cells. *ACS Nano* **2010**, *4*, 3374–3380.

(3) Chuang, C.; Brown, P.; Bulović, V.; Bawendi, M. Improved Performance and Stability in Quantum Dot Solar Cells through Band Alignment Engineering. *Nat. Mater.* **2014**, 1–6.

(4) Http://imagej.nih.gov/ij/.

(5) Böhm, M. L.; Kist, R. J. P.; Morgenstern, F. S. F.; Ehrler, B.; Zarra, S.; Kumar, A.; Vaynzof, Y.; Greenham, N. C. The Influence of Nanocrystal Aggregates on Photovoltaic Performance in Nanocrystal-Polymer Bulk Heterojunction Solar Cells. *Adv. Energy Mater.* **2014**, 1400139.

(6) Hassinen, A.; Moreels, I.; De Nolf, K.; Smet, P. F.; Martins, J. C.; Hens, Z. Short-Chain Alcohols Strip X-Type Ligands and Quench the Luminescence of PbSe and CdSe Quantum Dots, Acetonitrile Does Not. *J. Am. Chem. Soc.* **2012**, *134*, 20705–20712.

(7) Fritzinger, B.; Capek, R. K.; Lambert, K.; Martins, J. C.; Hens, Z. Utilizing Self-Exchange to Address the Binding of Carboxylic Acid Ligands to CdSe Quantum Dots. *J. Am. Chem. Soc.* **2010**, *132*, 10195–10201.

(8) Morris-cohen, A. J.; Malicki, M.; Peterson, M. D.; Slavin, J. W. J.; Weiss, E. A. Chemical, Structural, and Quantitative Analysis of the Ligand Shells of Colloidal Quantum Dots. *Chem. Mater.* **2013**, *25*, 1155.

(9) Anderson, N. C.; Hendricks, M. P.; Choi, J. J.; Owen, J. S. Ligand Exchange and the Stoichiometry of Metal Chalcogenide Nanocrystals: Spectroscopic Observation of Facile Metal-Carboxylate Displacement and Binding. *J. Am. Chem. Soc.* **2013**, *135*, 18536–18548.

(10) Srinivasan, U.; Mieyal, P. a.; Mieyal, J. J. pH Profiles Indicative of Rate-Limiting Nucleophilic Displacement in Thioltransferase Catalysis. *Biochemistry* **1997**, *36*, 3199–3206.

(11) Burris, S. C.; Zhou, Y.; Maupin, W. a.; Ebelhar, A. J.; Daugherty, M. W. The Effect of Surface Preparation on Apparent Surface pKa's of ??-Mercaptocarboxylic Acid Self-Assembled Monolayers on Polycrystalline Gold. *J. Phys. Chem. C* **2008**, *112*, 6811–6815.

(12) Vairavamurthy, M. a; Goldenberg, W. S.; Ouyang, S.; Khalid, S. The Interaction of Hydrophilic Thiols with Cadmium: Investigation with a Simple Model, 3-Mercaptopropionic Acid. *Mar. Chem.* **2000**, *70*, 181–189.

(13) Fey, N.; Ridgway, B. M.; Jover, J.; McMullin, C. L.; Harvey, J. N. Organometallic Reactivity: The Role of Metal–ligand Bond Energies from a Computational Perspective. *Dalton Trans.* **2011**, *40*, 11084.

(14) Jasieniak, J.; Califano, M.; Watkins, S. E. Size-Dependent Valence and Conduction Band-Edge Energies of Semiconductor Nanocrystals. *ACS Nano* **2011**, *5*, 5888–5902.

(15) Ip, A. H.; Thon, S. M.; Hoogland, S.; Voznyy, O.; Zhitomirsky, D.; Debnath, R.; Levina, L.; Rollny, L. R.; Carey, G. H.; Fischer, A.; *et al.* Hybrid Passivated Colloidal Quantum Dot Solids. *Nat. Nanotechnol.* **2012**, *7*, 577–582.

(16) Barreca, D. Nanostructured Cadmium Sulfide Thin Films by XPS. *Surf. Sci. Spectra* **2002**, *9*, 46.

(17) O`Connor, D. J.; Sexton, B. A.; Smart, R. *Surface Analysis Methods in Materials Science*; O'Connor, D. J.; Sexton, B. A.; Smart, R. S. C., Eds.; Springer Series in Surface Sciences; Springer Berlin Heidelberg: Berlin, Heidelberg, 2003; Vol. 23.

(18) Primera-Pedrozo, O. M.; Arslan, Z.; Rasulev, B.; Leszczynski, J. Room Temperature Synthesis of PbSe Quantum Dots in Aqueous Solution: Stabilization by Interactions with Ligands. *Nanoscale* **2012**, *4*, 1312–1320.